Green Chemistry

PAPER

View Article Online
View Journal | View Issue

Cite this: *Green Chem.*, 2015, **17**, 3378

Highly efficient nano-sized TS-1 with micro-/mesoporosity from desilication and recrystallization for the epoxidation of biodiesel with H_2O_2†

N. Wilde, M. Pelz, S. G. Gebhardt and R. Gläser*

Received 19th February 2015,
Accepted 15th April 2015

DOI: 10.1039/c5gc00406c

www.rsc.org/greenchem

The epoxidation of the unsaturated fatty acid methyl esters (FAME) in biodiesel with H_2O_2 was investigated at 323 K in the liquid phase over microporous nano-sized TS-1 as well as micro-/mesoporous nano-sized TS-1. Nano-sized TS-1 with stacked morphology exhibits a catalytic activity per number of Ti sites up to 30% higher than a conventional, industrial TS-1 catalyst. Mesoporosity was successfully introduced by a desilication-recrystallization approach. Desilication by alkaline treatment in the presence of the structure-directing agent tetrapropylammonium cation (TPA^+) or NaOH leads to the generation of undefined mesopores (10–40 nm), probably accompanied by an increase of the surface hydrophilicity. Consequently, the alkaline-treated materials show a two times lower catalytic activity in the epoxidation of biodiesel than the purely microporous parent material. The surfactant-assisted recrystallization of the alkaline-treated materials results in more uniform and smaller mesopores (3–10 nm). In the epoxidation, the recrystallized materials are remarkably more active with respect to both the purely microporous parent and alkaline-treated materials reaching a FAME conversion of 65% with an epoxide selectivity of 82%.

1. Introduction

Renewable feedstocks have recently gained considerable interest as raw materials for the production of chemicals. By far the largest share of utilized renewables in the chemical industry is held by fats and oils, since they offer widespread possibilities for different applications.[1] Vegetable oils represent one of the cheapest and most abundant biomass-based feedstock available in large quantities, and its use as starting material offers numerous advantages such as low toxicity and inherent biodegradability.[2] Among the applications of fats and oils, their conversion to fatty acid methyl esters (FAME) for biodiesel production is one of most prominent. FAME can be further converted to epoxidized fatty acid esters, which play an important role for a broad range of large-scale industrial syntheses of chemicals and intermediates such as plasticizers and stabilizers in PVC, intermediates in the production of polyurethane polyols or components for lubricants, cosmetics or pharmaceuticals.[1,3–7] Currently, the industrial-scale epoxidation of unsaturated fatty acid compounds is mainly carried out by the Prileshajew reaction with either pre- or *in situ* formed organic percarbonic acids.[8] This route suffers from several drawbacks: (i) the selectivity for epoxides is relatively low due to oxirane ring opening in the acidic reaction media, (ii) the handling of percarbonic acids and highly concentrated hydrogen peroxide solutions is strongly hazardous, and (iii) the aqueous solutions of C_1–C_3 carboxylic acids formed as by-products are strongly corrosive. Homogeneously and heterogeneously catalyzed epoxidations are the preferred alternatives to conventional stoichiometric routes. FAME epoxidation is mostly reported using organic hydroperoxides, such as *tert*-butyl- or cumene hydroperoxide, as epoxidizing agents.[9–11] However, hydrogen peroxide would be an economically and environmentally largely preferred oxidant.

The results from our previous work show that the epoxidation of unsaturated esters derived from the renewable raw material rapeseed oil methyl ester (RME), *i.e.*, biodiesel, can be accomplished over conventional titanium silicalite-1 (TS-1) with aqueous H_2O_2 as the sole oxidizing agent. Thus, biodiesel can be converted without additional purification and almost complete biodiesel conversion can be achieved after 24 h with an epoxide selectivity up to 80%. However, the conversion of fatty acid methyl esters over TS-1 is limited by mass-transfer

Institute of Chemical Technology, Universität Leipzig, Linnéstr. 03, 04103 Leipzig, Germany. E-mail: roger.glaeser@uni-leipzig.de; Tel: +49 341 9736300

† Electronic supplementary information (ESI) available: Figures for the BJH-PSD (Fig. S1) and conversion of biodiesel, epoxide selectivity and conversion of hydrogen peroxide as a function of reaction time (Fig. S2–S4). See DOI: 10.1039/c5gc00406c

within the catalyst particles, largely due to the size of its micropores with respect to the bulky FAME molecules.[12]

To overcome mass-transfer limitations in TS-1, intensive research has been carried out, focused on increasing the accessibility of active sites by decreasing the crystal size[13] or by incorporation of intra-crystalline mesoporosity. The first approach was shown to be feasible in our earlier work[12] using TS-1 with stacked morphology and crystals in the submicrometer scale. A goal of the present work was, thus, to further explore the potential of this approach by preparing nano-sized TS-1 catalysts, but different crystal sizes using different irradiation times during microwave-assisted synthesis.

The latter approach, *i.e.*, the incorporation of intra-crystalline mesoporosity into zeolite crystals, represents an elegant strategy, since in the corresponding catalysts the major advantages of micro- and mesoporous materials are combined. Several routes were reported to incorporate mesoporosity into TS-1, *e.g.*, by using amphiphilic organosilica zeolite precursors,[14,15] by utilizing hard templates[16–19] or by the top-down technique that involves the removal of silica *via* desilication by treatment in alkaline solutions.[20–23] However, mesopore introduction by desilication is poorly controllable with respect to, *e.g.*, size, shape, connectivity and location of the mesopores, and it often leads to a random and disordered mesopore system.

In contrast, several studies have demonstrated that a variety of different hierarchical zeolites with highly controlled mesoporosity can be obtained by a procedure involving zeolite desilication and recrystallization in the presence of a mesopore surfactant.[24] In these procedures, the degree of desilication is the most important parameter for tuning the structural and textural properties of recrystallized zeolites.

Despite the large number of reports on the synthesis, characterization and application of recrystallized MFI-type zeolites,[25] studies on the preparation of micro-/mesoporous TS-1 using the recrystallisation approach are rather scarce.[26,27] Another goal of the present work was, thus, devoted to the preparation of nano-sized TS-1 with stacked morphology and additional mesoporosity introduced by a two-step-approach including zeolite desilication by alkaline treatment and subsequent pseudomorphic transformation *via* recrystallization in the presence of the surfactant cetyltrimethylammonium cation ($CTMA^+$). One question was, thus, whether additional mesoporosity can be introduced into nano-sized TS-1 particles by desilication in alkaline media and in the presence of a aqueous basic solutions of the structure-directing agent, tetrapropylammonium cation (TPA^+). Furthermore, the influence of the desilication step on the properties of the recrystallized materials was systematically studied. In addition, the potential of the obtained materials for the heterogeneously catalyzed liquid-phase epoxidation of rapeseed oil methyl ester, *i.e.*, biodiesel, with aqueous H_2O_2 was investigated. In particular, the catalytic properties of the materials resulting from the desilication step on the one hand and from the recrystallization step on the other hand were compared.

2. Experimental section

2.1. Catalyst synthesis

Nano-sized titanium silicalite-1 with stacked morphology (TS-1_ns) was prepared according to Jin *et al.*[13] by microwave-assisted synthesis using tetraethyl orthosilicate (TEOS, >99%, Merck), tetrapropylammonium hydroxide (TPAOH, 10 wt% aqueous solution, Sigma Aldrich), titanium(IV) isopropoxide (TIP, 97%, Sigma Aldrich), isopropanol (99%, BDH Prolabo) and deionized water. Typically, TEOS (36.5 g), TPAOH solution (35.7 g) and deionized water (39.2 g) were mixed under stirring for 1 h. TIP (0.71 g) and isopropanol (8.15 g) were mixed under stirring in a separate beaker for 45 minutes. Subsequently, the solutions were combined and stirred, first for 2 h at room temperature and, then, at 353 K for 1 h to remove the isopropanol. The resulting mixture was separated into two parts of 42 cm^3 each, added to a 100 cm^3 PTFE autoclave and transferred to a microwave oven (MLS, Start 1500) for crystallization. For that purpose, the synthesis mixture was heated for 5 min with an irradiation power of 600 W to 438 K and held at this temperature under autogeneous pressure for 10 minutes (TS-1_ns10), 20 minutes (TS-1_ns20), 60 minutes (TS-1_ns60) and 70 minutes (TS-1_ns70), respectively. After cooling to room temperature, the obtained solids were recovered by centrifugation, washed five times with 25 cm^3 deionized water, dried at 393 K for 6 h and calcined in an air atmosphere at 823 K for 6 h.

Micro-/mesoporous TS-1 catalysts were obtained in two steps including a partial desilication of TS-1_ns in alkaline solution followed by a hydrothermal treatment for recrystallization in the presence of the structure-directing agent $CTMA^+$ (OH^-/Br^-). Desilication was carried out by alkaline treatment of the parent TS-1_ns70 with aqueous solutions of NaOH (≥98%, pellets, Sigma Aldrich) or NH_3 (25 wt% aqueous solution, AnalaR NORMAPUR, BDH Prolabo) partly in the presence of tetrapropylammonium cation TPA^+ (TPAOH, 10 wt% aqueous solution, Sigma Aldrich) as an additional structure-directing agent. In a typical preparation, 3 g of the parent TS-1_ns and 50 cm^3 of the alkaline solution, *i.e.*, 0.1 M NaOH, 0.1 M NaOH/1.0 M TPAOH or 13 M NH_3/1.0 M TPAOH) were transferred into a round-bottom flask (V = 100 cm^3) followed by heating under reflux to 338 K for 70 min. After cooling to room temperature, the solids were separated by centrifugation, washed with deionized water until neutral reaction of the washing water, dried at 358 K and calcined in air at 813 K for 5 h. The resulting materials are referred to as D_NaOH, D_NaOH/TPAOH, and D_NH_3/TPAOH, respectively.

For recrystallization, 1 g of the desilicated materials was mixed under stirring with an aqueous solution 21 cm^3 CTMAOH (0.08 M) and 21 cm^3 CTMABr (0.08 M). The CTMAOH solution was prepared by ion exchange of 1 g CTMABr (99%, Acros) dissolved in 42 cm^3 deionized water with 10 g Ampersep (900 OH, Fluka) at room temperature for 15 h. The resulting suspension was transferred to a polypropylene flask (Nalgene, V = 50 cm^3) and held at 383 K for 24 h. Then, the resulting solid was removed by filtration, washed

five times with 25 cm^3 deionized water and once with 20 cm^3 anhydrous ethanol (99%, BDH Prolabo), and dried in air at 363 K for 15 h. The obtained materials were calcined in air at 473 K for 2 h, at 673 K for 2 h and at 813 K for 15 h with a heating rate of 10 K min^{-1} between each of the steps. Depending on the preceding alkaline treatment, the recrystallized materials are labelled as R_DNaOH, R_DNaOH/TPAOH, and R_DNH$_3$/TPAOH, respectively.

An industrial sample of conventional titanium silicalite-1 (TS-1(ind.), powder) was supplied by Evonik Industries AG. Finally, all catalysts were pressed, crushed and sieved to obtain the grain size fraction between 50 and 150 μm for use in the catalytic experiments (*cf.* section 2.3).

2.2. Characterization

The catalysts were characterized by powder X-ray diffraction (XRD, Siemens D 5000) using CuKα-radiation (k = 0.15418 nm) in the 2θ-range of 1° and 80° with an angular step size of 0.05°.

Nitrogen sorption isotherms were recorded at 77 K using an ASAP 2000 (micromeritics) instrument. Samples were degassed in vacuum at 573 K for 10 h prior to measurement. The Brunauer–Emmett–Teller (BET) method was applied to determine the total specific surface area ($A_{S,BET}$) from the adsorption branch of the isotherm in the relative pressure range of p/p_0 = 0.01–0.10. The total specific pore volume was determined from the amount of nitrogen adsorbed at p/p_0 = 0.99. The specific micropore volume (V_{micro}) and mesopore volume (V_{meso}) as well as the specific macro- and mesopore surface area summarized as external specific surface area (S_{ext}) were determined with the t-plot method according to Lippens and de Boer.[28] The mesopore width distribution was calculated both from the adsorption and the desorption branch of the nitrogen sorption isotherm using the Barret–Joyner–Hallenda (BJH) model.

Diffuse reflectance UV–Vis (DR-UV–Vis) spectra were recorded at room temperature on a Perkin Elmer Lambda 650 S equipped with a 150 mm integrating sphere using spectralon® (PTFE, reflective value 99%) as a reference.

The titanium content of the samples was determined by elemental analysis *via* optical emission spectrometry with inductively coupled plasma (ICP-OES) after dissolving the solids in a mixture of HNO_3, HF and H_3BO_3 by chemical extraction under pressure.

Scanning electron microscopy (SEM) images were taken at 15 kV on a FEI Company Nova NanoLab 200 microscope with the samples sputtered with gold prior to measurement.

2.3. Catalytic experiments

Catalytic experiments were carried out batchwise in the liquid phase at 323 K in a two-necked round-bottom glass flask (V = 25 cm^3) with a septum for sampling and a reflux condenser with magnetic stirring (400 rpm) as described earlier.[12] Biodiesel (FAME, methyl oleate: 72 wt%, methyl linoleate + methyl linolenate: 19 wt%, rest: not determined; JCN Neckermann-Biodiesel GmbH Halle) was used as substrate, hydrogen peroxide (35 wt% aqueous solution, Solvay-Wolfen) as oxidant, acetonitrile (99.9%, BDH Prolabo) as a solvent and chlorobenzene (STD, 99.8%, Aldrich) as internal standard. In a typical experiment, 10 cm^3 solvent, 90 mg (0.30 mmol) FAME, 70 mg (1.44 mmol) hydrogen peroxide and 67 mg (0.6 mmol) chlorobenzene were mixed. The reaction was started by addition of the catalyst (150 mg) pre-treated in air at 373 K for 8 h. Samples taken periodically from the reaction mixture were diluted in acetonitrile and analyzed by capillary gas chromatography (Shimadzu GC 2010 equipped with a flame ionization detector).

The conversion in the epoxidation of biodiesel (FAME) was calculated as the ratio of the mass of converted unsaturated substrates, *i.e.*, methyl oleate, methyl linoleate and methyl linolenate, and their initial mass in the reactant mixture. The epoxide selectivity in FAME conversions is given as the cumulative mass of all epoxides (mono-, di- and tri-epoxides) formed relative to the converted mass of the substrates. As a measure for the catalyst efficiency, the FAME conversion was divided by the molar amount of titanium atoms present in the catalysts. The H_2O_2 conversion was calculated from the concentration of H_2O_2 in the initial reactant solution and in the product samples as determined by iodometric titration.

The experimental accuracy was within ±2% for the conversion of FAME, ±6% for the conversion of H_2O_2 and to ±5% for the epoxide selectivity, respectively.

3. Results and discussion

3.1. Catalysts

3.1.1. Nano-sized TS-1 with stacked morphology. As shown in Fig. 1, the powder XRD patterns of all nano-sized TS-1 materials exhibit reflections characteristic of the MFI framework topology. The single reflection at 2Θ = 24.35° indicates the change from monoclinic (silicalite) to the orthorhombic unit cell symmetry (TS-1). No significant intensity is observed for the reflection at 2Θ = 25.40, which is characteristic for crystalline titanium dioxide (TiO_2) in the anatase modification. Consequently, the presence of extra framework TiO_2 in the materials can be excluded.[29] Interestingly, the Ti-content of the materials can be adjusted by the irradiation time during microwave-assisted synthesis and increases with increasing irradiation time. Thus, TS-1_ns10 possesses 0.45 wt% Ti, TS-1_ns20 0.52 wt%, TS-1_ns60 0.65 wt% and TS-1_ns70 0.90 wt% Ti, respectively (*cf.* Table 1). This implies that the Ti content is higher in the outer shell of the TS-1 crystallites with respect to the inner core.

SEM images of the nano-sized TS-1 catalysts (TS-1_ns) from microwave-assisted synthesis for different irradiation times are shown in Fig. 2. All samples exhibits puck-like crystals of submicrometer size and a stacked morphology through connection of the crystals on top of one another along their [010] direction. As reported previously, this stacking is sufficiently robust and a result of strong chemical bonds between the crystals.[13] In contrast to results reported by Jin *et al.*,[13] the stacked

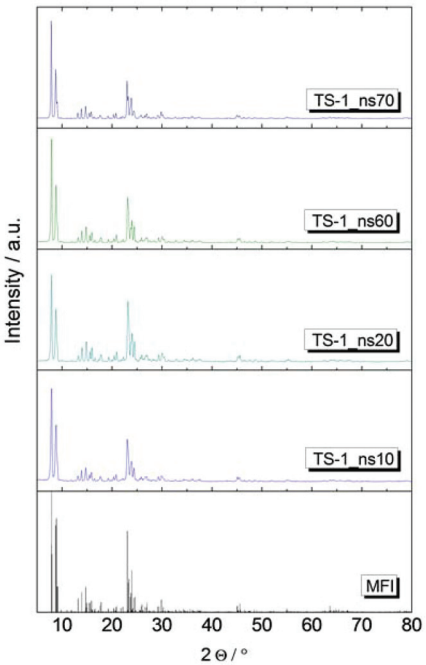

Fig. 1 Powder X-ray diffraction patterns of the TS-1_ns obtained after different irradiation times during microwave-assisted synthesis. The MFI-diffraction pattern is adapted from ref. 40.

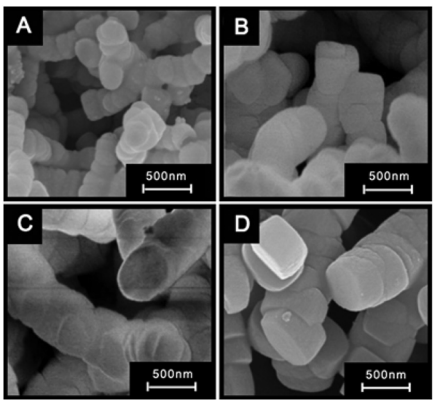

Fig. 2 SEM images of nano-sized TS-1_ns from microwave-assisted synthesis with different irradiation times of 10 min (A, TS-1_ns10), 20 min (B, TS-1_ns20), 60 min (C, TS-1_ns60) and 70 min (D, TS-1_ns70).

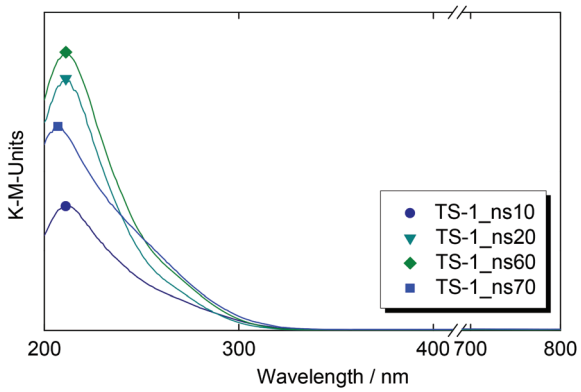

Fig. 3 DR-UV–Vis spectra (in Kubelka–Munk (K–M)-units) of nano-sized TS-1_ns obtained after different irradiation times during microwave-assisted synthesis.

morphology observed here was already obtained after an irradiation time of 10 minutes. The size of the crystals noticeably increases with irradiation time up to 60 minutes during microwave-assisted synthesis, whereas no significant increase of the particle size is observed for irradiation times longer than 60 minutes. To gain direct information about the nature and coordination of the Ti-species, the pre-dried materials were characterized by DR-UV–Vis spectroscopy. For all TS-1_ns catalysts from microwave-assisted synthesis, a band with a maximum centered at 210 nm is observed (Fig. 3). This band is characteristic of a O(2p) > Ti(3d) charge transfer transition, and is generally assigned to isolated, tetrahedrally coordinated $Ti(OSi)_4$ species in hydrophobic zeolite frameworks.[30] Nevertheless, TS-1_ns obtained after an irradiation time of 10 minutes shows a line width at half maximum (LWHM) of *ca.* 60 nm indicating the simultaneous presence of tetrahedral tripodal $Ti(OSi)_3OH$ and/or loosely coordinated tetrapodal

Table 1 Titanium content and textural properties of nano-sized TS-1_ns, desilicated (D-series) and recrystallized TS-1 (R_D-series)

	ω_{Ti}[a]/wt%	V_{micro}[b]/cm^3 g^{-1}	$V_{3-10\ nm}$[c]/cm^3 g^{-1}	$V_{10-40\ nm}$[c]/cm^3 g^{-1}	A_{micro}[b]/m^2 g^{-1}	A_{ext}[b]/m^2 g^{-1}	$A_{S,BET}$[d]/m^2 g^{-1}
TS-1_ns10	0.46	0.17	n.d.	n.d.	327	46	373
TS-1_ns20	0.52	0.18	n.d.	n.d.	320	3	323
TS-1_ns60	0.65	0.17	n.d.	n.d.	323	7	330
TS-1_ns70	0.90	0.20	n.d.	n.d.	420	13	433
D_NH_3/TPAOH	1.00	0.13	0.04	0.11	280	78	358
D_NaOH/TPAOH	1.20	0.11	0.02	0.12	245	50	290
D_NaOH	1.10	0.12	0.06	0.03	270	133	403
R_DNH_3/TPAOH	1.10	0.13	0.13	0.05	248	235	483
R_DNaOH/TPAOH	1.30	0.18	0.15	0.05	258	245	503
R_DNaOH	1.20	0.14	0.07	0.04	305	138	443

[a] From ICP-OES. [b] t-plot-de Boer. [c] BJH. [d] BET. n.d. not determined.

$Ti(OSi)_4$ Ti species.[30] By increasing the irradiation time during microwave-assisted synthesis up to 60 minutes, the LWHM of the DR-UV–Vis bands decrease, which leads to the conclusion that TS1_ns20 and TS-1_ns60 possess less tetrahedral tripodal $Ti(OSi)_3OH$ and loosely coordinated $Ti(OSi)_4$ species than TS-1_ns10. TS-1_ns70 exhibits also a broader LWHM than TS-1_ns20 and TS-1_ns60, respectively. Obviously, the irradiation time during microwave-assisted synthesis plays a key role for the incorporation of Ti into the framework.

Low-temperature nitrogen sorption isotherms for the nano-sized TS-1 catalysts are shown in Fig. 4. All samples exhibit a reversible type I isotherm (according to the IUPAC classification) with a steep rise at relative pressures $p/p_0 < 0.01$, confirming their microporous character, although having an enhanced nitrogen uptake at higher relative pressures $p/p_0 > 0.9$. The uptake increases with increasing irradiation time during microwave-assisted synthesis and is most pronounced for the material obtained after 70 minutes. The uptake ($p/p_0 > 0.9$) is uncommon for microcrystalline TS-1 and can be attributed to the stacked morphology (*cf.* SEM-image, Fig. 2), *i.e.*, the existence of larger mesopores between the stacked nano-sized crystallites. Additionally, a step in nitrogen adsorption isotherm at $p/p_0 = 0.1–0.2$ is observed. This can be explained by the "fluid-to-crystalline" like phase transition of the adsorbed phase inside the micropores.[31] This step does not indicate "real" porosity, but corresponds to a false peak in the PSD with a maximum at aprox. 2 nm.[31]

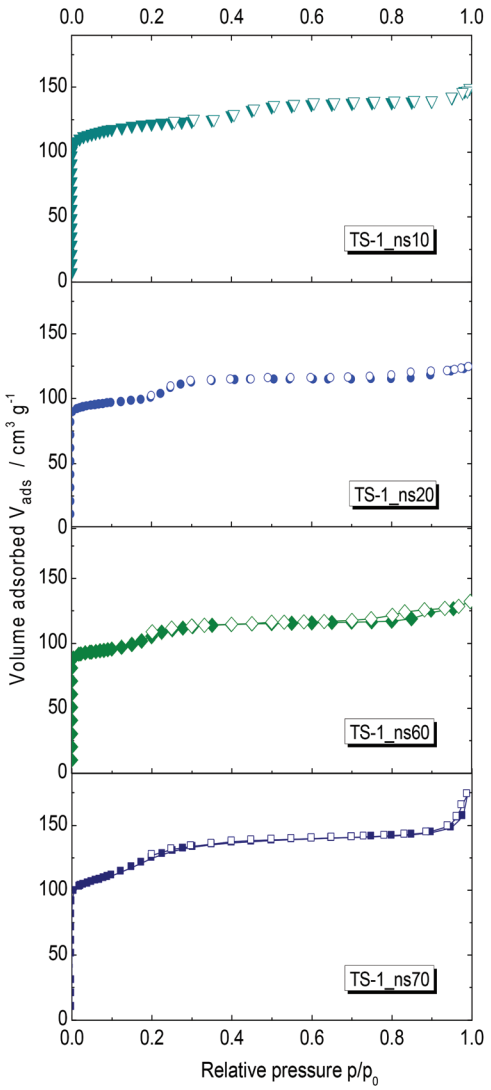

Fig. 4 Nitrogen adsorption (closed symbols) and desorption (open symbols) isotherms of nano-sized TS-1_ns obtained after different irradiation times of 10 min, 20 min, 60 min and 70 min during microwave-assisted synthesis.

3.1.2. Nano-sized TS-1 with micro-/mesoporosity from desilication and recrystallization. In case of both the desilicated and recrystallized materials, the XRD patterns show clear evidence of the presence of the MFI structure (Fig. 5). However, in comparison to the parent TS-1_ns70, a significant reduction in the intensity of the diffraction reflections is observed for all desilicated materials. This can be explained based on the attack of Si–O–Si or Si–O–Ti bonds by the hydroxide anions of the alkaline solution causing partial disrupture of the crystal framework and, thus, lower long-range order in the materials.

The recrystallized materials show a relative degree of crystallinity comparable to or even slightly higher than that of the parent TS-1_ns70 material. In agreement with the literature,[25] this effect can be attributed to the recovery of zeolitic phase due to the healing of defects within the framework during recrystallization. Moreover, amorphous material generated during desilication may have been dissolved.[25]

The small-angle XRD patterns (not shown) point to the absence of any structured mesoporous phase in the recrystallized materials.

Elemental analysis (Table 1) of both the filtrate and the solids confirm the preferential leaching of Si, leading to a slightly increased Ti-content in the alkaline-treated and recrystallized materials. Note, however, that the Ti-contents in the desilicated and recrystallized materials are comparable.

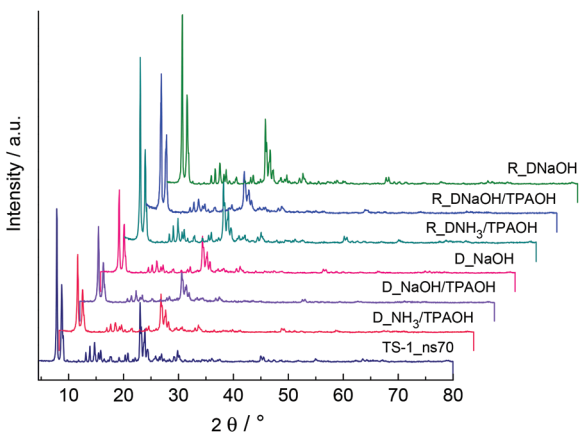

Fig. 5 Powder X-ray diffraction patterns of the parent TS-1_ns70, desilicated (D-series) and recrystallized TS-1 (R_D-series).

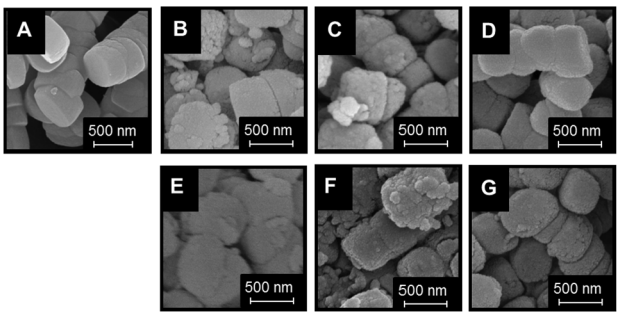

Fig. 6 SEM images of the parent TS-1_ns70 (A), desilicated (D-series) TS-1: D_NH_3/TPAOH (B), D_NaOH/TPAOH (C), D_NaOH (D) (upper part) and recrystallized TS-1 (R_D-series): R_DNH_3/TPAOH (E), R_DNaOH/TPAOH (F), R_DNaOH (G) (lower part).

Scanning electron microscopy of the desilicated materials show that all materials possess an increased surface roughening due to the introduction of additional porosity as proven by results from nitrogen sorption (*cf.* Table 1). The overall size of the crystals as well as the stacked morphology are virtually not affected by the alkaline treatment (D-series, Fig. 6). The crystal size and morphology also remain unaffected after the recrystallization step (R_D-series, Fig. 6).

The TS-1 samples obtained by alkaline treatment in the presence of the structure-directing agent TPA^+ exhibit debris with diameter of aprox. 50 nm on the external surface of the crystallites (Fig. 6B and C). TS-1_ns70 treated with pure NaOH did not show such deposition of debris (Fig. 6D). This strongly suggests that during the alkaline treatment silica is dissolved from the framework, while in the presence of TPA^+ a partial restructuring of dissolved silica and deposition of debris occurs. A recrystallization of TS-1 in the presence of TPA^+ was described by Wang *et al.*[20] although under different conditions.

For the desilicated materials, a broader band is observed in the DR-UV-Vis spectra between 200 and 300 nm with a maximum centered at *ca.* 220 nm (Fig. 7). Compared to the parent TS-1_ns70, which possesses a line width at half maximum (LWHM) of approximately 40 nm, the band width increases and the maximum shifts to higher wavelengths. After recrystallization, the position of the band maximum (around 220 nm) remains practically unchanged, while the LWHM slightly increases with respect to the desilicated materials. The red shift of the maximum to 220 nm in both the desilicated and the recrystallized materials suggests the simultaneous presence of tetrahedral tripodal $Ti(OSi)_3OH$ and loosely coordinated tetrapodal $Ti(OSi)_4$ Ti-species in higher amounts than in the parent TS-1_ns70.[30] Moreover, the band spread is characteristic of Ti-containing mesoporous silicas such as Ti-MCM-41 and can be attributed to the simultaneous presence of isolated Ti-atoms in tetra, penta- or hexahedral coordination.[32] For D_NaOH and R_DNaOH LWHM is much broader than for the materials treated with TPAOH during desilication. However, the absence of bands above 300 nm for all materials suggests that non-desired extra-framework TiO_2 phases related to the anatase structure are not present. This observation is in good agreement with results from XRD (see above).

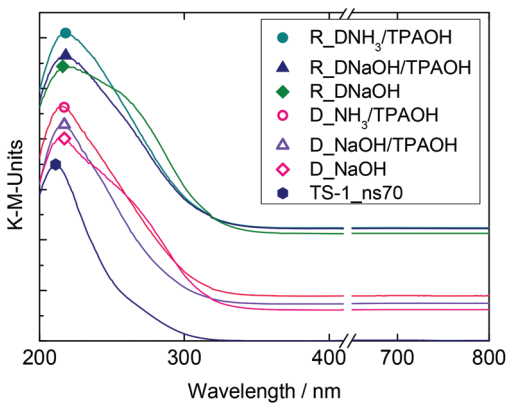

Fig. 7 DR-UV-Vis spectra (in Kubelka–Munk units) of the parent TS-1_ns70, desilicated (D-series) and recrystallized TS-1 (R_D-series).

Alkaline treatment of TS-1_ns70 leads to nitrogen sorption isotherms representing combined type I and type II behavior. A remarkably enhanced uptake of nitrogen occurs at higher relative pressures of $p/p_0 = 0.85$, which is more pronounced for the materials treated in the presence of TPAOH (Fig. 8B and C). While the material treated with pure NaOH shows only a slightly pronounced hysteresis, the presence of TPAOH during desilication results in the development of a distinct H2 type hysteresis loop. The forced closure of the hysteresis loop for both D_NH_3/TPAOH and D_NaOH/TPAOH is due to a sudden drop in the volume adsorbed along the desorption branch in the range of p/p_0 = 0.41–0.50. This phenomenon is often referred to as the "Tensile Strength Effect" (TSE).[31] Furthermore, the shape of the nitrogen adsorption-isotherm with the steep closing of the hysteresis loop is typical for mesoporous systems with pore openings considerably smaller than diameter of the inner pores, *e.g.*, for ink-bottle shaped pores or partially constricted interconnected porous systems. For such a pore geometry, the cavitation mechanism of emptying the mesopores leads to sudden release of the adsorbate when its partial pressure is below a certain critical value.[31,33]

In case of the occurrence of TSE phenomena, the application of the BJH model to the desorption branch of the isotherm leads to a completely different result compared to that obtained from the adsorption branch, which is hardly affected by TSE (*cf.* ESI, Fig. S1†). The pore size distribution (PSD) obtained from nitrogen desorption isotherms are dominated by narrow peaks with maxima at about 3.9 nm, respectively, while this peak is absent in the PSD calculated from the adsorption branches. Therefore, the analysis of nitrogen adsorption isotherms is recommended.[31] Taking into account the BJH-PSD from adsorption branches of nitrogen isotherms of desilicated TS-1 catalysts, the presence of undefined mesopores and a broad pore-diameter distribution in the range of 10–40 nm is confirmed. It should be noted, however, that,

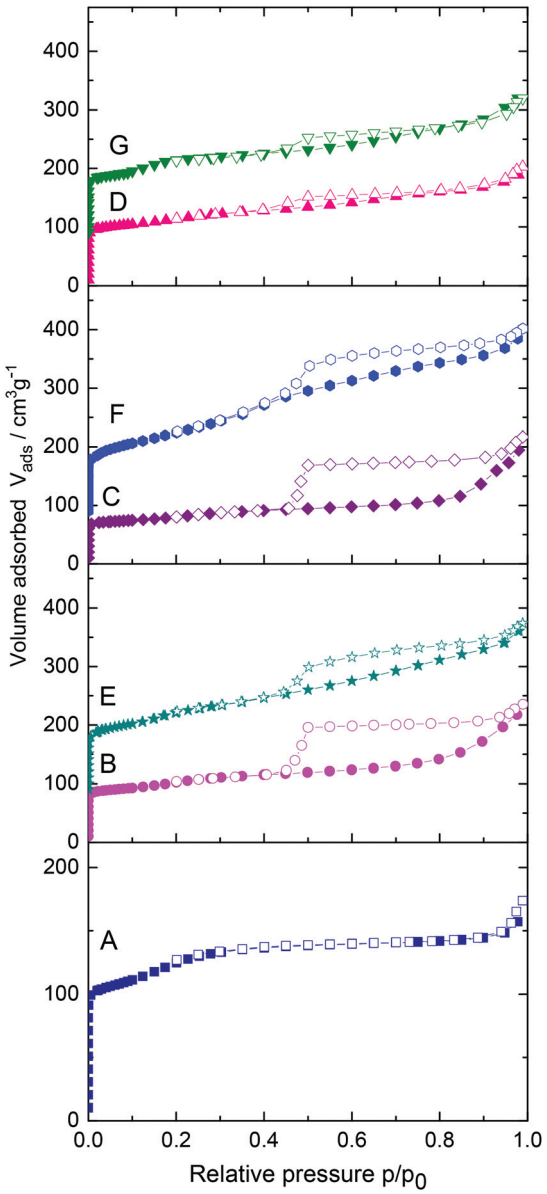

Fig. 8 Nitrogen adsorption (closed symbols) and desorption (open symbols) isotherms of the parent TS-1_ns (A), desilicated TS-1_D: D_NH_3/TPAOH (B), D_NaOH/TPAOH (C), D_NaOH (D) and recrystallized TS-1_R: R_DNH_3/TPAOH (E), R_DNaOH/TPAOH (F), R_DNaOH (G). For clarity isotherms for recrystallized materials TS-1_R were vertically displaced by 80 cm^3 g^{-1}, respectively.

since the adsorption isotherms correspond to the metastable adsorption state, the corresponding pore diameter distributions are also not quite reliable.[33]

Upon recrystallization of the desilicated TS-1 materials (D-series) in the presence of the surfactant cation CTA^+, the shape of the nitrogen adsorption isotherms in the recrystallized materials (R_D-series) is unchanged and also displays a combined type I and type II behavior (Fig. 8). In contrast to desilicated materials, however, the enhanced nitrogen uptake in the relative pressures range of p/p_0 = 0.3–0.8 is more pronounced and indicates the presence of smaller mesopores (3–10 nm) after recrystallization. This finding is in good agreement with the substantially enhanced contribution of the mesopore volume in the range of 3–10 nm (Table 1). Moreover, the hysteresis loops of the recrystallized TS-1 materials are less pronounced than that of the desilicated materials and can be assigned to a combined H2 and H4 type.

Values of the specific BET surface area as well as the micro- and mesopore volume determined with the t-plot-de Boer method[28,34] are summarized in Table 1. It must be kept in mind that the specific surface area calculated by the BET-model is not valid for materials, which contain a substantial amount of microporosity, and hence can only be regarded as a BET-equivalent surface area for comparative purposes.[35,36]

The parent TS-1_ns70 possesses a specific BET surface area of 433 m^2 g^{-1} which is in excellent agreement with values previously reported for nano-sized TS-1 with stacked morphology ($A_{S,BET}$ = 398 m^2 g^{-1}).[13] Furthermore, 13 m^2 g^{-1} is contributed by the external surface area from t-plot analysis, *i.e.*, surface area from the true external crystal surfaces and from internal voids larger than micropores due to the stacked morphology.

Upon alkaline treatment of the parent TS-1_ns70 in the presence of TPA^+, a significantly increased amount of mesoporosity with diameters of 10–40 nm is developed, *i.e.*, $V_{10–40\ nm}$ = 0.11 cm^3 g^{-1} for D_NH_3/TPAOH and $V_{10–40\ nm}$ = 0.12 cm^3 g^{-1} for D_NaOH/TPAOH, respectively. The mesopore formation by selective silicon removal is accompanied by a reduction of the micropore volume of aprox. 45% with respect to the parent TS-1_ns70 (Table 1).

Surprisingly, while no substantial mesopore formation is observed for the material from treatment with aqueous NaOH solution only (D_NaOH, $V_{3–10\ nm}$ = 0.06 cm^3 g^{-1}, $V_{10–40\ nm}$ = 0.03 cm^3 g^{-1}), the external surface area on this material is highest (A_{ext} = 133 m^2 g^{-1}) among all desilicated samples. The absence of a pronounced hysteresis loop in the nitrogen sorption isotherm of this material supports that the relatively high value of A_{ext} is due to contributions of intercrystalline rather than to intracrystalline mesoporosity. In contrast, the specific BET surface area is strongly decreased for D_NH_3/TPAOH (358 m^2 g^{-1}) and D_NaOH/TPAOH (295 m^2 g^{-1}) with respect to the parent TS-1_ns70, which can be directly attributed to the high contribution of mesopore volume in the range of 10–40 nm.

The recrystallized materials exhibit specific BET surface areas of 483 m^2 g^{-1} for R_DNH_3/TPAOH and 503 m^2 g^{-1} for R_DNaOH/TPAOH, *i.e.*, 130 and 200 m^2 g^{-1} higher than that of the starting material from desilication. More remarkably, 235 m^2 g^{-1} (R_DNH_3/TPAOH) and 245 m^2 g^{-1} (R_DNaOH/TPAOH) are from the external surface for the recrystallized materials, respectively. These values are about three and five times higher than that of the respective TS-1 from desilication. They can be directly related to the increased specific mesopore volume in the diameter range of 3–10 nm ($V_{3–10\ nm}$ = 0.13/0.15 cm^3 g^{-1} *vs.* 0.04/0.02 cm^3 g^{-1}, Table 1) and provide proof of the surfactant-assisted recrystallization as described by Garcia-Martinez *et al.*[24] for zeolite Y. These authors suppose

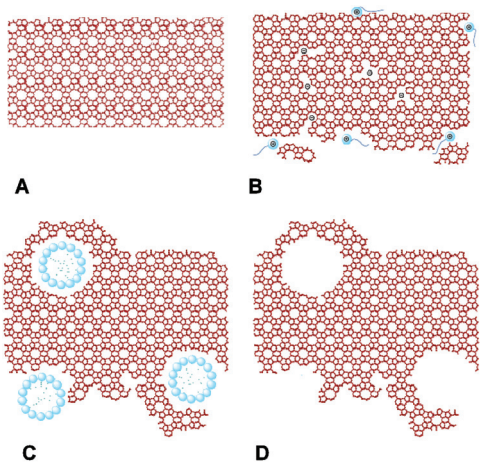

Fig. 9 Proposed mesopore formation process in TS-1: (A) parent purely microporous TS-1, (B) Si–O–Si/Si–O–Ti bond opening and reconstruction in alkaline media, (C) crystal rearrangement to accommodate the surfactant micelles and (D) removal of the template to expose the mesoporosity introduced.[24]

that the surfactant cations form micelles within the zeolite crystals and cause a structural rearrangement to generate uniform mesopores around the micelles. Accordingly, a scheme for the introduction of controlled mesoporosity into crystalline microporous materials through a surfactant-assisted crystal rearrangement mechanism for TS-1 is proposed in Fig. 9.

3.2. Epoxidation of Biodiesel with H_2O_2

In order to minimize acid-catalyzed secondary products, acetonitrile was chosen as the solvent for the conversion of biodiesel (FAME) with H_2O_2 over the TS-1-based catalysts. Because of its slightly basic nature, it was shown before that it supports the formation of epoxides and hinders the formation of undesired side-products.[12] In Fig. 10, the reaction scheme for the epoxidation of methyloleate, *i.e.*, the major compound in biodiesel, with H_2O_2 in acetonitrile over TS-1 is shown. Besides the major product methyl 9,10-epoxy stearate (typically with a selectivity of $S > 80\%$), several side-products are formed, predominantly in consecutive reactions (Fig. 10). The product from acid-catalyzed hydrolysis, methyl 9,10-dihydroxy stearate, and the products from oxidative cleavage of the epoxide are present in about equal amounts. Ketones derived from rearrangement are formed in negligible amounts only ($S < 1\%$). The amount of detected cleavage products increases with reaction time. However, the exact amount of the side-products was not further quantified.

Recently, it was reported for the epoxidation of methyloleate with H_2O_2 in acetonitrile at 358 K that the epoxide formation can occur through an uncatalyzed Payne-type oxidation.[37] Since, however, no FAME conversion was observed in the absence of a catalyst ($V_{acetonitrile}$ = 10 cm^3, c_{FAME} =

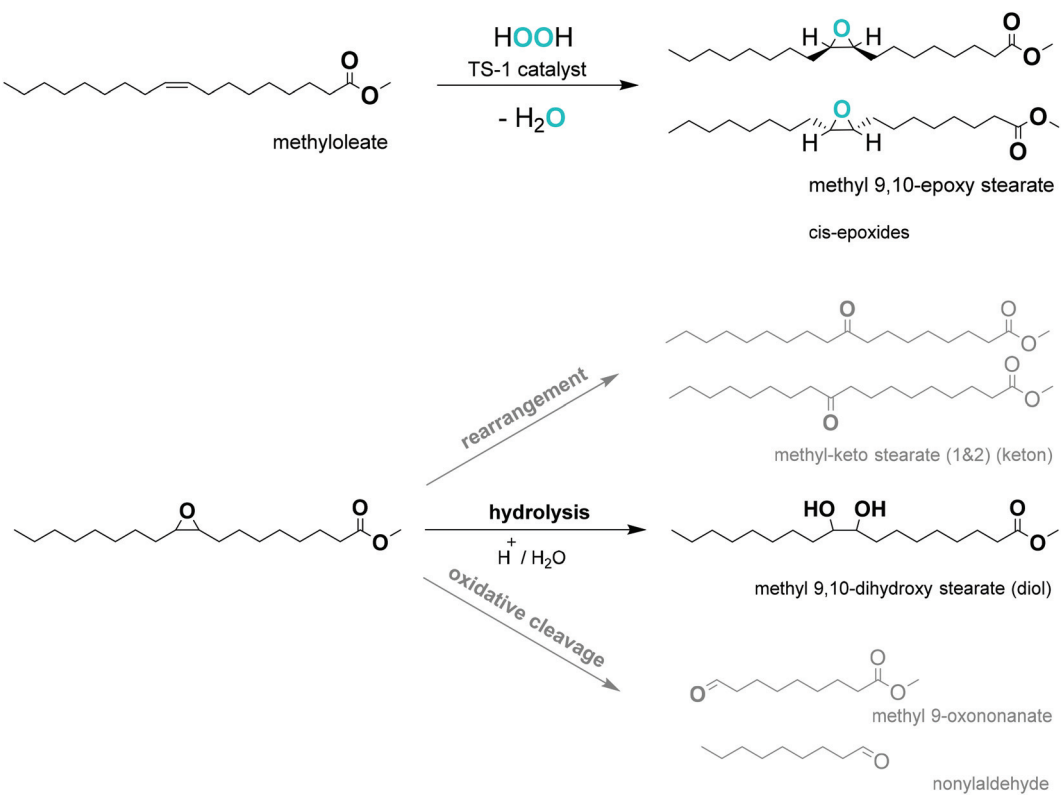

Fig. 10 Proposed reaction scheme for the epoxidation of methyloleate with H_2O_2 over TS-1.

0.03 mol l^{-1}, ($n_{H_2O_2}/n_{FAME}$) = 5 mol mol^{-1}, T = 323 K), a significant contribution of uncatalyzed oxidation pathways can be excluded under the conditions applied in the present study.

3.2.1. Conversion over nano-sized TS-1 with stacked morphology. Fig. 11 shows the results of the epoxidation of FAME with H_2O_2 over nano-sized TS-1 with different crystallite sizes. By increasing the irradiation time during microwave-assisted synthesis, the activity of the nano-sized TS-1 catalysts for the epoxidation increases (see Fig. 2). While over the catalyst obtained after 10 minutes irradiation time (TS-1_ns10) a catalyst efficiency, *i.e.*, FAME conversion relative to the number of Ti atoms present in the catalyst, of 0.8% μmol^{-1} is achieved, the catalyst efficiency increases with particles size and amounts to 1.18% μmol^{-1} and 1.20% μmol^{-1} for TS-1_ns20 and TS-1_ns60, respectively. Interestingly, TS-1_ns70 is less active and the catalyst efficiency is close to that of TS-1_ns10. Previously, it was reported that the formation of the stacked morphology through condensation of hydroxyl groups on the crystal surface is accompanied by an increase of the surface hydrophobicity with increasing microwave-irradiation time.[13] More FAME molecules are adsorbed on the more hydrophobic surface, so that the concentration of adsorbed reactants in close proximity of the active Ti sites is higher leading to a higher catalytic activity per Ti site. This explanation is supported by the observations from DR-UV–Vis spectroscopy from which we conclude that TS-1_ns10 and TS-1_ns70 have a higher density of Ti(SiO_3)OH-species on the surface (*cf.* Fig. 7). Note also that the Ti content on the outer shell of the nano-sized TS-1 catalysts increases with increasing particle size (*cf.* section 3.1, Table 1) leading to a higher density of accessible active Ti sites. The epoxide selectivity (S_{eFAME}) follows a similar trend. It increases from 42% (TS-1_ns10) to 68% (TS-1_ns20) and 77% (TS-1_ns60).

While the eFAME selectivity increases for the catalyst from the longest microwave-irradiation (TS-1_ns70), its catalytic efficiency is lower than that of the other catalysts with stacked morphology. This might be due to either a too high density of active Ti sites on the surface which cannot be fully utilized by the adsorbed large FAME molecules or a hindrance of access to the active Ti sites as a result of closer stacking of the TS-1 crystallites. Interestingly, both catalyst efficiency and eFAME selectivity of TS-1_ns70 are comparable to those for the conventional industrial catalyst TS-1 (ind.). Thus, TS-1_ns70 was chosen as parent material for the post-synthetic modification by the introduction of mesoporosity.

3.2.2. Conversion over nano-sized TS-1 with micro-/mesoporosity. As shown above, the selective desilication of framework Si leads to the introduction of mesopores (*cf.* section 2.1). It has previously been reported that mesopores are highly beneficial for improving the efficiency for phenol hydroxylation over alkaline treated TS-1 catalysts.[23] However, over the desilicated TS-1 catalysts prepared in the present study, the catalyst efficiency for biodiesel conversion was less than 0.40% μmol^{-1} and, thus, significantly lower compared to the parent microporous TS-1_ns70 (0.87% μmol^{-1}) (Fig. 13). Likewise, the epoxide selectivity is up to 20% lower than that for TS-1_ns70. This lower epoxide selectivity is mainly due to the formation of diols resulting from acid-catalyzed hydrolysis of the epoxide (*cf.* Fig. 10). The generation of larger mesopores by desilication is accompanied by a considerable development of external surface area and a partial damage of the framework of the crystals. This generates hydroxyl groups (Fig. 12) and increases the hydrophilicity of the catalyst surface. A similar observation was reported by Cheneviere *et al.*[14] and Sanz *et al.*[38] who successfully prepared hierarchically structured TS-1 in the presence of amphiphilic organosilanes. In both studies, it was found that the hierarchical TS-1 exhibits a lower activity than purely

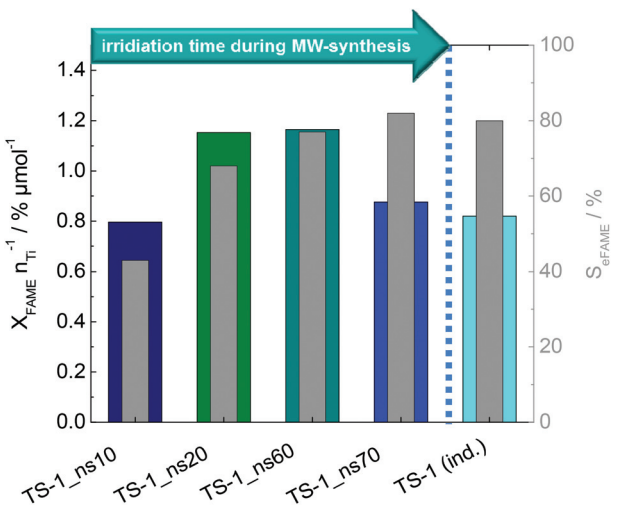

Fig. 11 Catalyst efficiency (conversion related to the amount of Ti atoms in the catalysts) for the epoxidation of biodiesel (FAME) with H_2O_2 as well as epoxide selectivity (S_{eFAME}) over nano-sized TS-1 and conventional TS-1(ind.) after 5 h of reaction ($V_{acetonitrile}$ = 10 cm^3, c_{FAME} = 0.03 mol L^{-1}, ($n_{H_2O_2}/n_{FAME}$) = 5 mol mol^{-1}, $m_{cat.}$ = 150 mg, T = 323 K).

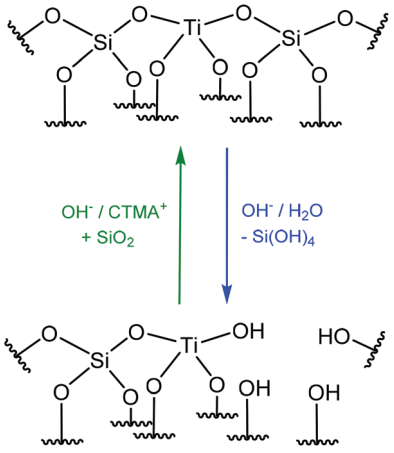

Fig. 12 Generation of defect sites (surface hydroxyl groups) in TS-1 by desilication (blue), "healing" of the defects by re-arrangement in the presence of $CTMA^+$ (green).

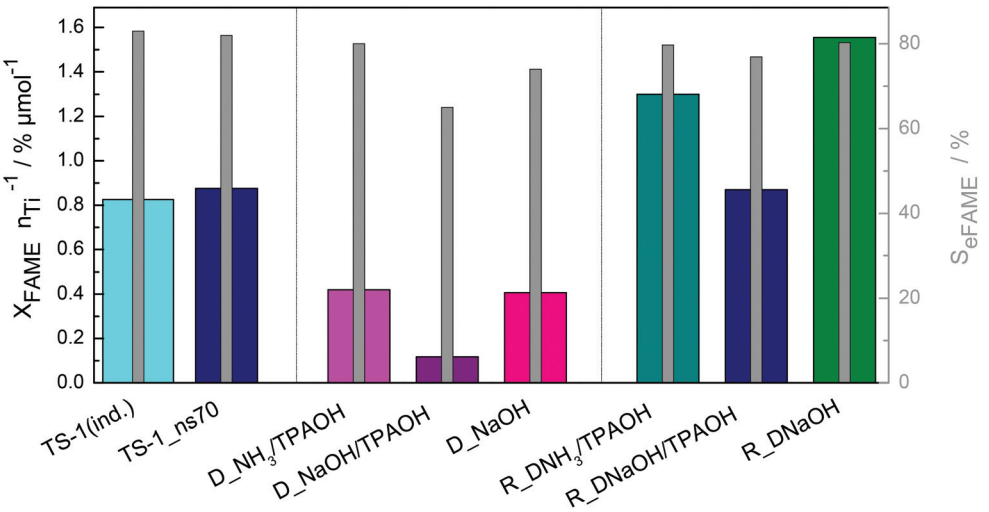

Fig. 13 Catalyst efficiency (conversion related to the amount of Ti atoms in the catalysts) for the epoxidation of biodiesel (FAME) with H_2O_2 over micro-/mesoporous TS-1 as well as epoxide selectivity (S_{eFAME}) after 5 h of reaction ($V_{acetonitrile}$ = 10 cm^3, c_{FAME} = 0.03 mol L^{-1}, ($n_{H_2O_2}/n_{FAME}$) = 5 mol mol^{-1}, m_{cat} = 150 mg, T = 323 K).

microporous TS-1 in the epoxidation of olefins when H_2O_2 is used as the oxidant. This was explained by the hydrophilic nature of the hierarchically structured materials as a result of a high surface hydroxyl group density associated to the secondary porosity. The beneficial effect of surface hydrophobicity on the activity, selectivity and lifetime of TS-1-based catalysts for the epoxidation of alkenes with aqueous H_2O_2 solution was proven in several studies (see ref. 39 for a review).

Comparing the desilicated TS-1 materials and taking into account that the catalyst desilicated by only NaOH (D_NaOH) is more hydrophilic than those obtained by alkaline treatment in the presence of TPA cations, one can conclude that the ink-bottle shaped or the partially constricted interconnected pores as present in D_NaOH/TPAOH and D_NH$_3$/TPAOH are responsible for the lower catalytic activity rather than a slightly higher hydrophilicity. These textural properties of the catalysts desilicated in the presence of TPAOH may hinder access to the active Ti sites when compared to the catalysts from desilication with NaOH only.

Recrystallization of the desilicated materials results in a significantly higher catalytic activity with respect to the desilicated and the parent TS-1_ns70 materials (Fig. 13). Over the recrystallized catalysts, the values for the catalyst efficiency of 1.29% µmol^{-1} (R_DNH$_3$/TPAOH), 1.05% µmol^{-1} (R_DNaOH/TPAOH) and 1.58% µmol^{-1} (R_DNaOH) are three to four times higher than those of the parent analogues before recrystallization. Also the epoxide selectivity is as high as for the initial catalyst (TS-1_ns70) before any modification. In particular, the catalysts from recrystallization after desilication with NaOH (R_DNaOH) show the highest catalyst efficiency with an approx. two times higher conversion per number of Ti-sites than the parent TS-1_ns70. Note also that the activity of the other two catalysts obtained after recrystallization relative to R_DNaOH is the same as after desilication, *i.e.*, the catalytic efficiency of R_DNH$_3$/TPAOH is higher than that of R_DNaOH/TPAOH.

Evidently, the active Ti sites in the recrystallized TS-1 catalysts (R_D-series) are more readily accessible for the reactant molecules with respect to the alkaline-treated ones. This can be attributed to a more uniform distribution of mesopores observed in the recrystallized materials. Such mesopores would also facilitate removal of epoxide molecules from the catalyst surface before undergoing consecutive reactions to undesired side-products. This is in accordance with the higher epoxide selectivity observed for the recrystallized compared to the desilicated materials. In addition, the recrystallization probably leads to a healing of defects, *e.g.*, a condensation of silanol groups on the catalyst surface generated during the alkaline treatment. This, then, results in an increased hydrophobic character of the catalyst surface (Fig. 12). Support for this conclusion is supplied by XRD results which confirms that recrystallized materials possess a higher degree of crystallinity than the desilicated ones and the parent TS-1_ns70.

4. Conclusions

In order to improve the accessibility of Ti sites in TS-1 catalysts, nano-sized TS-1 catalysts with stacked morphology and different particle sizes were prepared by microwave-assisted synthesis. By increasing the microwave-irradiation time of the synthesis gel up to 60 minutes, the activity of the TS-1 catalysts for the epoxidation of biodiesel with H_2O_2 was enhanced. Furthermore, nano-sized TS-1 exhibits a catalytic activity per Ti site up to 30% higher than a conventional TS-1(ind.) catalyst. By applying a two-step desilication–recrystallization treatment, mesoporosity was successfully incorporated into the nano-sized TS-1 catalysts.

Irregularly shaped mesopores in the range of 10–40 nm with reduced accessibility incorporated by desilication have a negative impact on the catalytic activity. Thus, over the desilicated catalysts, the catalytic activity per active Ti site and epoxide selectivity were strongly reduced compared to the purely microporous TS-1. More uniform mesopores as present in the recrystallized TS-1 materials are most beneficial for the catalytic activity. Thus, the catalytic activity per active Ti site is up to two times higher with respect to the initial untreated TS-1 and the epoxide selectivity reaches 82%.

In addition to a balanced degree of micro- and mesoporosity as well as a uniform shape and accessibility of larger pores, the hydrophobic/hydrophilic surface properties of the catalysts have to be considered. The quantitative assessment of the surface hydrophobicity and its relationship to hierarchical porosity and catalytic performance are attractive goals for future research. The clarification of these relations may significantly contribute to further improve the catalytic activity, selectivity and stability of TS-1-based catalysts for alkene epoxidation.

Acknowledgements

The authors are grateful to Prof. Dr. W.-D. Einicke, Institute of Chemical Technology, Universität Leipzig, for his assistance with measuring the nitrogen sorption isotherms. Thanks are also due to Dipl.-Phys. Jörg Lenzner, Institute of Experimental Physics II, Universität Leipzig, for conducting the SEM investigations.

Notes and references

1 U. Biermann, U. Bornscheuer, M. A. R. Meier, J. O. Metzger and H. J. Schafer, *Angew. Chem., Int. Ed.*, 2011, **50**, 3854–3871.
2 U. Biermann, W. Friedt, S. Lang, W. Luhs, G. Machmuller, J. O. Metzger, M. R. Klaas, H. J. Schafer and M. P. Schneider, *Angew. Chem., Int. Ed.*, 2000, **39**, 2206–2224.
3 F. D. Gunstone and F. B. Padley, in *Epoxidiesed oils*, ed. F. D. Gunstone, Marcel Dekker, New York, 1997, p. 759.
4 A. Campanella, E. Rustoy, A. Baldessari and M. A. Baltanas, *Bioresour. Technol.*, 2010, **101**, 245–254.
5 R. D. Kulkarni, P. S. Deshpande, S. U. Mahajan and P. P. Mahulikar, *Ind. Crops Prod.*, 2013, **49**, 586–592.
6 Z. S. Petrovic, L. T. Yang, A. Zlatanic, W. Zhang and I. Javni, *J. Appl. Polym. Sci.*, 2007, **105**, 2717–2727.
7 E. Del Rio, M. Galia, V. Cadiz, G. Lligadas and J. C. Ronda, *J. Polym. Sci., Part A: Polym. Chem.*, 2010, **48**, 4995–5008.
8 M. Guidotti, N. Ravasio, R. Psaro, E. Gianotti, L. Marchese and S. Coluccia, *Green Chem.*, 2003, **5**, 421–424.
9 M. A. Camblor, A. Corma, P. Esteve, A. Martinez and S. Valencia, *Chem. Commun.*, 1997, 795–796.
10 M. Guidotti, R. Psaro, N. Ravasio, M. Sgobba, E. Gianotti and S. Grinberg, *Catal. Lett.*, 2008, **122**, 53–56.
11 M. Guidotti, N. Ravasio, R. Psaro, E. Gianotti, S. Coluccia and L. Marchese, *J. Mol. Catal. A: Chem.*, 2006, **250**, 218–225.
12 N. Wilde, C. Worch, W. Suprun and R. Glaser, *Microporous Mesoporous Mater.*, 2012, **164**, 182–189.
13 H. L. Jin, N. Z. Jiang, S. M. Oh and S. E. Park, *Top. Catal.*, 2009, **52**, 169–177.
14 Y. Cheneviere, F. Chieux, V. Caps and A. Tuel, *J. Catal.*, 2010, **269**, 161–168.
15 D. Serrano, R. Sanz, P. Pizarro and I. Moreno, *Chem. Commun.*, 2009, 1407–1409.
16 Y. C. Zou, S. G. Wei and X. J. Qu, *Chem. J. Chin. Univ.*, 2008, **29**, 1926–1929.
17 Q. Zhao, P. Li, D. Q. Li, X. G. Zhou, W. K. Yuan and X. J. Hu, *Microporous Mesoporous Mater.*, 2008, **108**, 311–317.
18 P. Birke, P. Kraak, R. Pester, R. Schodel and F. Vogt, *Zeolites Microporous Crystals*, 1994, **83**, 425–432.
19 Y. M. Fang and H. Q. Hu, *Catal. Commun.*, 2007, **8**, 817–820.
20 Y. R. Wang, M. Lin and A. Tuel, *Microporous Mesoporous Mater.*, 2007, **102**, 80–85.
21 S. T. Tsai, P. Y. Chao, T. C. Tsai, I. K. Wang, X. X. Liu and X. W. Guo, *Catal. Today*, 2009, **148**, 174–178.
22 A. Silvestre-Albero, A. Grau-Atienza, E. Serrano, J. Garcia-Martinez and J. Silvestre-Albero, *Catal. Commun.*, 2014, **44**, 35–39.
23 P. Y. Chao, S. T. Tsai, T. C. Tsai, J. B. Mao and X. W. Guo, *Top. Catal.*, 2009, **52**, 185–192.
24 J. Garcia-Martinez, M. Johnson, J. Valla, K. H. Li and J. Y. Ying, *Catal. Sci. Technol.*, 2012, **2**, 987–994.
25 I. I. Ivanova and E. E. Knyazeva, *Chem. Soc. Rev.*, 2013, **42**, 3671–3688.
26 Y. Zhu, Z. L. Hua, X. X. Zhou, Y. D. Song, Y. Gong, J. Zhou, J. J. Zhao and J. L. Shi, *RSC Adv.*, 2013, **3**, 4193–4198.
27 Y. Zuo, W. C. Song, C. Y. Dai, Y. P. He, M. L. Wang, X. S. Wang and X. W. Guo, *Appl. Catal., A*, 2013, **453**, 272–279.
28 J. H. de Boer, B. C. Lippens, B. G. Linsen, J. C. Broekhof, A. Vandenhe and T. J. Osinga, *J. Colloid Interface Sci.*, 1966, **21**, 405–411.
29 Y. G. Li, Y. M. Lee and J. F. Porter, *J. Mater. Sci.*, 2002, **37**, 1959–1965.
30 P. Ratnasamy, D. Srinivas and H. Knozinger, *Adv. Catal.*, 2004, **48**, 1–169.
31 J. C. Groen, L. A. A. Peffer and J. Perez-Ramirez, *Microporous Mesoporous Mater.*, 2003, **60**, 1–17.
32 S. Gontier and A. Tuel, *Zeolites*, 1995, **15**, 601–610.
33 M. Thommes, *Chem. Ing. Tech.*, 2010, **82**, 1059–1073.
34 P. Voogd, J. J. F. Scholten and H. Vanbekkum, *Colloids Surf.*, 1991, **55**, 163–171.
35 M. Thommes, B. Smarsly, M. Groenewolt, P. I. Ravikovitch and A. V. Neimark, *Langmuir*, 2006, **22**, 756–764.
36 K. S. W. Sing, D. H. Everett, R. A. W. Haul, L. Moscou, R. A. Pierotti, J. Rouquerol and T. Siemieniewska, *Pure Appl. Chem.*, 1985, **57**, 603–619.

37 M. Guidotti, E. Gavrilova, A. Galarneau, B. Coq, R. Psaroa and N. Ravasio, *Green Chem.*, 2011, **13**, 1806–1811.
38 R. Sanz, D. P. Serrano, P. Pizarro and I. Moreno, *Chem. Eng. J.*, 2011, **171**, 1428–1438.
39 R. Gläser and J. Weitkamp, in *Handbook of Porous Solids*, ed. F. Schüth, K. S. W. Sing and J. Weitkamp, Wiley-VCH, Weinheim, 2002, pp. 395–431.
40 H. van Koningsveld, J. C. Jansen and H. van Bekkum, *Zeolites*, 1990, **10**, 235–242.